ACS APPLIED MATERIALS & INTERFACES

Research Article

www.acsami.org

Simple Control of Surface Topography of Gold Nanoshells by a Surfactant-less Seeded-Growth Method

Antonio Topete,[†] Manuel Alatorre-Meda,[‡] Eva M. Villar-Álvarez, Adriana Cambón, Silvia Barbosa,* Pablo Taboada,* and Víctor Mosquera

Grupo de Física de Coloides y Polímeros, Departamento de Física de la Materia Condensada, Universidad de Santiago de Compostela, Santiago de Compostela 15782, Spain

Supporting Information

ABSTRACT: We report the synthesis of branched gold nanoshells (BGNS) through a seeded-growth surfactant-less method. This was achieved by decorating chitosan-Pluronic F127 stabilized poly(lactic-*co*-gycolic) acid nanoparticles (NPs) with Au seeds (NP-seed), using chitosan as an electrostatic self-assembling agent. Branched shells with different degrees of anisotropy and optical response were obtained by modulating the ratios of $HAuCl_4/K_2CO_3$ growth solution, ascorbic acid (AA) and NP-seed precursor. Chitosan and AA were crucial in determining the BGNS size and structure, acting both as coreductants and structure directing growth agents. Preliminary cytotoxicity experiments point to the biocompatibility of the obtained BGNS, allowing their potential use in biomedical applications. In particular, these nanostructures with "hybrid" compositions, which combine the features of gold nanoshells and nanostars showed a better performance as surface enhanced Raman spectroscopy probes in detecting intracellular cell components than classical smoother nanoshells.

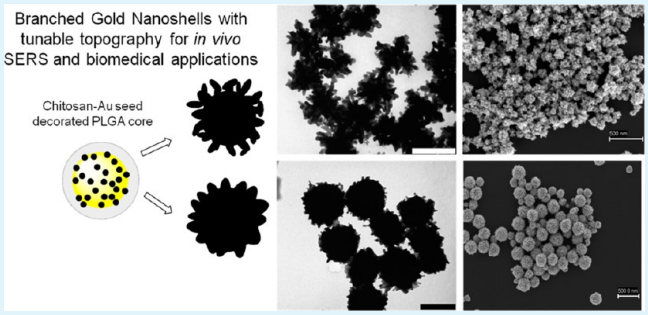

KEYWORDS: *hybrid nanoparticles, nanoshells, surfactant-less synthesis, controlled topography, surface enhanced Raman scattering, cell viability*

1. INTRODUCTION

Obtaining metal nanoparticles (NPs) through highly efficient and controlled synthetic methodologies has been a very active area of research during the past two decades due to their unique size- and shape-dependent properties.[1−3] In particular, gold (Au) NPs exhibit remarkable optical properties due to their localized surface plasmon resonance (LSPR) absorption with peak positions that are largely dependent on the NP size, shape, composition and the dielectric constant of the medium.[4] Also, the strong electromagnetic field generated by LSPR excitation can drastically enhance the fluorescence and Raman signals of nearby molecules.[5−7] Hence, all these extraordinary properties have increased the potential applications of these nanoscaled materials in different fields such as in catalysis,[8,9] photonics,[10,11] sensing[12,13] or nanomedicine,[14,15] among others.

Au NPs have been produced to different shapes, such as spheres,[16,17] rods,[18,19] prisms,[20] cubes,[21] plates,[22] nanoshells,[23] hollow[24] and branched[25] NPs. Nonspherical NPs and nanoshells can exhibit, for example, important shifts of their LSPR bands to the red and near-infrared region (NIR) of the electromagnetic spectrum. Thanks to their great energy absorption capabilities, they can generate considerable heat under red and near-infrared (NIR) radiation, becoming excellent photothermal agents; they possess unique catalytic and surface enhanced Raman spectroscopy (SERS) properties in comparison to spherical NPs due to the their larger surface area, more availability of reactive metal sites and the anisotropic distribution of the electromagnetic field near their surface, respectively. In addition to the former properties, the hollow architecture of Au nanoshells also enables the encapsulation of different cargo molecules to provide further functionalities, which opens up their special utility in the fields of diagnosis and therapy.[26,27]

On the other hand, both theoretical calculations and experimental data indicate that a large electromagnetic field enhancement exists at the tips of branched particles, leading to stronger SERS and photothermal activities, provided that their larger specific surface areas facilitate a higher photohermal transduction efficiencies and an easier penetration of the electric field in comparison to smoother nanostructures.[28,29]

Hence, the combination of a branched surface structure and cargo loading capability in a single nanostructure can open the door to develop a new class of exciting multifunctional nanomaterials for sensing and biomedical applications. In this regard, Halas et al. have synthesized nanoshells with a roughened surface by treating presynthesized nanoshells with

Received: February 17, 2014
Accepted: June 24, 2014
Published: June 24, 2014

an aqueous solution containing cetyltrimethylammonium bromide (CTAB), $HAuCl_4$ and ascorbic acid (AA) followed by chemical etching of the presynthesized nanoshells.[30,31] However, this methodology did not give rise to highly surface anisotropic structures, and the far-field scattering properties of these roughened nanoshells were similar to those of smoothed ones except for small differences in the angular light scattering distributions; in addition, the used postsynthesis chemical etching approach is not ideal because it can lead to particle destabilization and does not allow control of the surface topography. To solve this issue, very recently, Park et al. developed a high yield synthetic method to radially arranged gold spikes on the surface of polymeric NPs, the so-called "spiky nanoshells".[32,33] The synthetic procedure is based on the CTAB-assisted seed-growth method[29,30] on negatively charged polymer templates in the presence of silver (Ag) ions. This methodology leads to Au nanospikes organized at a radial position determined by the size of the polymer template. The presence of CTAB and/or metal halide salts, in particular NaBr, plays a key role in the formation and regulation of the spiky shell morphology.[34] However, this process has still several drawbacks as (i) the use of toxic cationic surfactants (CTAB) during the particle synthesis, which can be a severe problem for intended biomedical applications if their full elimination is not completely achieved; or (ii) it is composed of several reduction steps, i.e., the reduction of deposited Ag ions on the polymeric template surface by $NaBH_4$, followed by the CTAB-assisted growth of branches/spikes on the Ag seeds by reduction of an Au growth solution by AA, and subsequent exploitation of the preferential binding of bromide ions (from CTAB) to selective facets of Au NPs.[35]

Here, we report an alternative methodology to synthesize branched gold nanoshells (BGNS) in high yield based on a simpler seed-reduction method. In this approach, preformed citrate-stabilized Au seeds were attached on the surface of chitosan-Pluronic F127 stabilized poly(lactic-*co*-gycolic) acid (PLGA) NPs and subsequently anisotropically grown by the addition of a growth solution exclusively composed of Au salt, potassium carbonate (K_2CO_3) and AA. By altering the feeding ratio of different raw components, the structure of the anisotropic metal nanoshells can be tuned and, as a consequence, their associated optical properties too. Finally, the biocompatibilty of the as-obtained nanoshells was tested in vitro to decipher future use in biological applications as biomedical nanoplatforms. Also, a preliminary test of the SERS detection capability of intracellular components of the present spiky nanoshells was performed and compared to that of smoother nanoshells.

2. MATERIALS AND METHODS

2.1. Materials. Poly(D,L-lactic-*co*-glycolic) (PLGA) of 40−75 kDa with a 50:50 lactide−glycolide ratio, Pluronic F127, hydrogen tetrachloroaureate(III) trihydrate ($HAuCl_4{\cdot}3H_2O$), low molecular weight chitosan (LMW-chitosan, M_W = 111 kDa), potassium carbonate anhydrous, sodium borohydride, sodium citrate tribasic, resazurin (7-hydroxy-3*H*-phenoxazin-3-one 10-oxide) and ascorbic acid were purchased from Sigma-Aldrich (St. Louis, MO, USA). ProLong Gold antifade reagent with DAPI, Dulbecco's modified Eagle medium, fetal bovine serum (FBS), L-glutamine, penicillin/streptomycin, sodium pyruvate and MEM nonessential amino acids (NEAA) were purchased from Invitrogen (Carlsbad, USA). Dialysis membrane tubing (molecular weight cutoff ~ 3500) was purchased from Spectrum Laboratories, Inc. (Rancho Dominguez, California). Thiol-PEG (HS-PEG, molecular weight 5000 Da was from Polymer Source (Ontario, Canada). All other chemicals and solvents were of reagent grade (purchased from Sigma-Aldrich). Milli-Q water was used for all aqueous solutions. All glassware was washed with aqua regia and HF 5% (v/v) and extensively rinsed with water.

2.2. Preparation of PLGA NPs. PLGA NPs were synthesized by a nanoprecipitation method with modifications. Briefly, a 10% (w/v) solution of PLGA in acetone was added dropwise at a flow ratio of 0.166 mL/min to 50 mL of a cooled (10 °C, 1% (w/v) aqueous solution of F127 copolymer (PEO_{98}−PPO_{67}−PEO_{98}) under moderate magnetic stirring (250 rpm). Then, the resulting emulsion was homogenized with a tip sonicator (at 100 W, 20 kHz Bandelin SonoPuls, Bandelin Electronic GmbH, Berlin, Germany) for 10 min in an ice cold bath. The emulsion was magnetically stirred for 4 h and then centrifuged in 10 mL tubes at 9000 rpm for 30 min at 18 °C. The resulting pellets were dispersed in 5 mL of water, stirred for 4 h, centrifuged and dispersed again under the same conditions. The final PLGA NP dispersion was translucent and homogeneous with hydrodynamic size and ζ-potential of 110 ± 20 nm and −39 ± 7 mV, respectively.

2.3. Synthesis of Au Seed NPs. Citrate-capped gold seeds were prepared based on a method previously reported by Jana et al.[18] Briefly, 10 mL of 0.026 mM trisodium citrate was mixed with 0.125 mL of 0.010 M $HAuCl_4{\cdot}3H_2O$. Next, 0.3 mL of 0.1 M ice cold $NaBH_4$ solution was added and the solution mixed. The solution turned orange-pink immediately, indicating particle formation. The seed dispersion was aged overnight to allow for decomposition of unreacted $NaBH_4$. The average particle size obtained from transmission electron microscopy (TEM) was 3 ± 1.5 nm.

2.4. Preparation of NP-Seed Precursor. PLGA NPs have a negative surface charge (ca. −40 mV) due to the carboxyl groups of PLGA chains. We used chitosan, a natural biocompatible polycation, to reverse the surface charge of NPs to positive and allow the subsequent attachment of negatively charged Au seeds. Briefly, 5 mL of PLGA NPs (~4×10^{11} NPs/mL) was mixed with 1.25 mL of 1% (w/v) chitosan (in 1% (v/v) acetic acid) and the mixture was stirred for 4 h at room temperature, followed by centrifugation at 9000 rpm for 30 min at 18 °C and subsequent dispersion in 25 mL of water. The ζ-potential of chitosan-coated PLGA NPs was +15 ± 6 mV. Then, 25 mL of Au seeds (~1×10^{14} NPs/mL) was added and the mixture was stirred for 4 h, followed by centrifugation at 7000 rpm for 20 min at 18 °C. The supernatant was discarded and the pellets were dispersed in 25 mL of water. The NP-seed dispersion was sonicated (20 W, 20 kHz) for 5 s to avoid any kind of particle aggregation. The final NP-seed concentration was calculated to be ca. 4.0×10^{11} NP/mL. Control samples without chitosan as the seed-attaching element were prepared by mixing 4 mL of PLGA NPs with 21 μM cysteamine, 21 μM EDC and 21 μM sulfo-NHS. This mixture was reacted for 4 h followed by centrifugation at 9000 rpm for 30 min and 18 °C and subsequent dispersion in 2 mL of water. Twenty milliliters of citrate-capped seeds were added. Incubation and washing steps were the same as those of NP-chitosan-seeds samples.

2.5. Preparation of Au Growth Solution. Au growth solution was prepared by dissolving 0.05 g of K_2CO_3 in 98 mL of water. After 30 min of stabilization, 2 mL of 0.025 M $HAuCl_4{\cdot}3H_2O$ was added and the solution aged for 24 h. The solution had a pH = 9.87 right before the synthesis. At this pH, the predominant species of Au are $[AuCl_x(OH)_{4-x}]^-$ (x = 0−4), with predominance of $[Au(OH)_4]$.[36] The final concentration of Au^{3+} in the growth solution was 0.6 mM.

2.6. Branched Gold Nanoshell Growth (BGNS). To ensure homogeneous BGNS sizes, NP-seed precursor was first filtered with 1.2 μm filters (Merck Millipore, MA, USA) to eliminate large aggregates formed during centrifugation. In a typical synthesis, 0.5 mL of NP-seed precursor was mixed with 2.5 mL of the Au growth solution under moderate stirring (400 rpm) at 25 °C. After 1 min, 5 to 75 μL of fresh 0.5 M AA (pH = 1.95) was added and the reaction volume brought to 6.5 mL. After a few seconds, the mixture changed from colorless to blue, indicating the formation of branched nanoshells. A similar procedure was followed when changing the NP-seed and the Au growth solution concentrations by adding different volumes of the stock solution (from 0.01 to 3 mL depending

Scheme 1. Growth of Branched Gold Nanoshells on PLGA NPs Using Chitosan or Cysteamine as Binding Linkers for Au Seeds

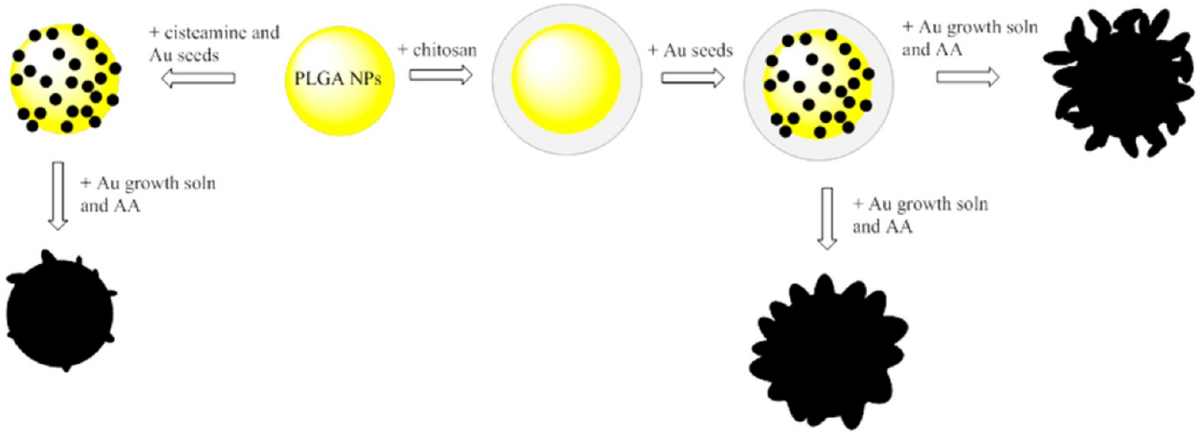

on conditions, see below). After completion of the reduction reaction, and in order to ensure water stability for long time, thiolated polyethylene glycol was linked to the surface of the nanoshells. Briefly, BGNS (optical density ~ 1), K_2CO_3 (20 mM) and SH-PEG-OCH_3 (0.5 mM) were mixed in a volume ratio of 2:1:2. The conjugation was carried out at 4 °C for 4 h under moderate stirring. Pegylated BGNS were centrifuged at 3500 rpm for 15 min at 20 °C to eliminate free SH-PEG-OCH_3, and subsequently dispersed in water.

2.7. Particle Characterization. Dynamic light scattering (DLS) measurements were performed at 25 °C by means of an ALV-5000F (ALV-GmbH, Germany) instrument with λ = 488 nm wavelength, scattering angle to incident beam was θ = 90° and sampling time 120 s. The ζ-potential measurements were performed at 25 °C in a Zetasizer Nano ZS (Malvern Instruments, UK) using folded capillary disposable cells and measured by triplicate. UV−vis spectroscopy measurements were performed in a CARY 100 Bio UV−visible (Agilent Technologies, Santa Clara, USA) spectrophotometer. UV−vis spectra of BGNS were recorded 30 min after the growth reaction without dilution if not otherwise stated. UV−vis kinetic experiments were recorded with a sampling time of 5 s at 25 °C. Transmission electron microscopy (TEM) images of PLGA NPs and BGNS were obtained with a Philips CM-12 (Philips, The Netherlands) microscope operating at 120 kV. HR-TEM images and selected area electron diffraction (SAED) patterns were obtained with a transmission electron microscope (Carl-Zeiss Libra 200 FE-EFTEM, Germany) operating at 200 kV. Scanning electron microscopy (SEM) images were obtained with a FESEM Ultra Plus (Zeiss, Germany) microscope operating at 20 kV. X-ray diffraction (XRD) experiments were carried out with a rotating anode X-ray generator (Siemens D5005, Germany). Twin Göbel mirrors were used to produce a well-collimated beam of Cu Kα radiation (λ = 1.5418 Å). X-ray diffraction patterns were recorded with an imaging plate detector (AXS F.Nr. J2−394). The gold concentration in solution was determined by inductively coupled plasma-mass spectrometry (ICP-MS) in a Varian 820-MS instrument (Agilent Technologies, USA). The number of Au NS was calculated assuming a sphere model of 200 nm in diameter. For corroboration, the BGNS concentration was also calculated by the following equation which is derived from Beer's law:

$$\frac{\text{nanoshells}}{\text{mL}} = \frac{2.303 \cdot A_{\text{peak}}}{\sigma_{\text{ext}} \cdot b} \quad (1)$$

where A_{peak} is the experimental absorption at the peak plasmon resonance wavelength, σ_{ext} is the theoretical extinction cross section at the peak plasmon resonance wavelength taken from Mie theory (~2×10^{12} M^{-1} cm^{-1}) and b is the path length of the cuvette used, in centimeters.

2.8. Cell Nanoparticle Uptake. BGNS uptake was followed by confocal microscopy by seeding HeLa cells on poly-L-lysine coated glass coverslips (12 × 12 mm) placed inside 6-well plates (3 mL, 1.5×10^5 cells/well) and grown for 24 h at standard culture conditions, that is, 5% CO_2 at 37 °C) in Dulbecco's modified Eagle medium (DMEM) supplemented with 10% (v/v) FBS, 2 mM L-glutamine, 1% penicillin/streptomycin, 1 mM sodium pyruvate and 0.1 mM MEM non-essential amino acids (NEAA). Then, 400 μL of NP solution (1×10^9 NPs/mL) in PBS was added to cells. After 6 h of incubation, the NP-containing cells were washed three times with PBS pH 7.4 and then fixed with paraformaldehyde 4% (w/v) for 10 min and washed with PBS. Samples were visualized with an oil immersion 63× objective (NA 1.4) using a DMI6000B Leica microscope (Leica Microsystems, Germany) in differential interference contrast (DIC) mode.

Uptake of BGNS by HeLa cells was also investigated by TEM. HeLa cells were seeded in 6-well plates (3 mL, 1.5×10^5 cells/well) and grown for 24 h at standard culture conditions. Then, 400 μL (1×10^9 NPs/mL) were added to cells. After 6 h of incubation, the NP-containing cells were washed three times with PBS, trypsinized and centrifuged at 1500 rpm for 4 min. Cell pellets were fixed with 500 μL of 2.5% (v/v) glutaraldehyde. The pellet was then included in agar, postfixed with osmium tetraoxide in 0.1 M cacodylate buffer (1% (w/v)) and finally pelletized with Eponate (Ted Pella Inc., Redding, CA, USA). Ultrathin cuts were obtained with an ultramicrotome (UltraCut S, Leica, Germany) and were analyzed by TEM (JEOL JEM 1011, Japan).

2.9. Resazurin Cell Cytotoxicity Assay. HeLa cells were seeded in a 96-well-plate at 15 000 cells/well (3 wells/sample) in 100 μL growth medium (Dulbecco's modified Eagle medium (DMEM) supplemented with 10% fetal bovine serum (FBS), 2 mM L-glutamine, 1% penicillin/streptomycin, 1 mM sodium pyruvate and 0.1 mM MEM non-essential amino acids (NEAA). After 24 h, cells were incubated for 6 h with 50 μL of BGNS at different concentrations and some cells were left without BGNS as a control (blank). Then, cells were washed with PBS and a solution out of 10% (v/v) of resazurin (Sigma-Aldrich) and 90% of growth medium was added to each well (100 μL/well) and incubated for 3 h. Fluorescence spectra were recorded with a microplate fluorescence spectrometer (FluoroLog-3, Horiba, Japan). Spectra were recorded by exciting at 560 nm and recording fluorescence emission in the range 572−650 nm. The background signal (640−650 nm) was subtracted to the average maximal fluorescence of each sample. Values were normalized and plotted against concentration in logarithmic scale.

2.10. Surface-Enhanced Raman Spectroscopy. SERS measurements were done with cells grown on quartz coverslips (0.2 mm) and incubated with media containing 1×10^{10} NP/mL of either smooth or spiky nanoshells for 6 h. To confirm a relative similar amount of nanoshells internalized by cells, NP-containing cells were washed three times with PBS, trypsinized, counted and digested in 0.5 mL of aqua regia (one part 100% HNO_3 to three parts 100% HCl). Each sample volume was made up to 5 mL with distilled water, and the gold content was determined by inductively coupled plasma-mass spectrometry (ICP-MS) in a Varian 820-MS instrument (Agilent Technologies, USA).

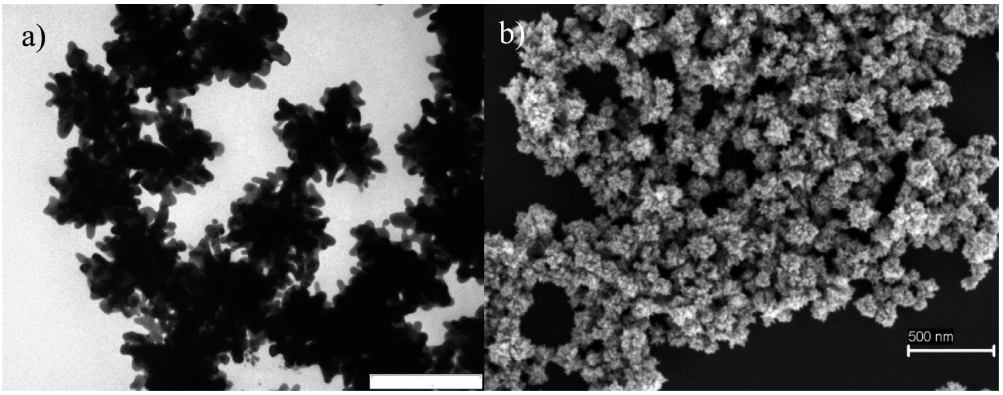

Figure 1. a) TEM images of BGNS with spikes protruding from the core (AA solution =5 μL (0.5 M), Au growth solution =2.5 mL, and NP-seeds solution =0.5 mL). b) SEM image showing the high yield production of BGNS and negligible undesired byproducts. Scale bar is 200 nm in a) and 500 nm in b).

Raman spectra were measured upon excitation with a 785 nm laser line to avoid cell damage. Inelastically scattered light was collected with a Renishaw Invia Reflex system, equipped with a confocal optical microscope, high resolution gratings (1200 g mm^{-1}), a two-dimensional CCD detector and an x,y,z motorized stage with 100 nm of resolution. Spectra were collected by focusing the laser line onto the sample, using a 100× objective (N.A. 0.95), which provided a spatial resolution of about 1 nm^2, with accumulation times of 5 s and laser power at the sample of 5 mW. Bulk Raman spectra of cells with no nanoshells were acquired with a laser intensity of 75 mW and 120 s acquisition times and averaged on more than 50 cells and background corrected.

3. RESULTS AND DISCUSSION

The current synthesis of BGNS involved the preparation of Au seed-decorated PLGA NPs (NP-seed) and subsequent

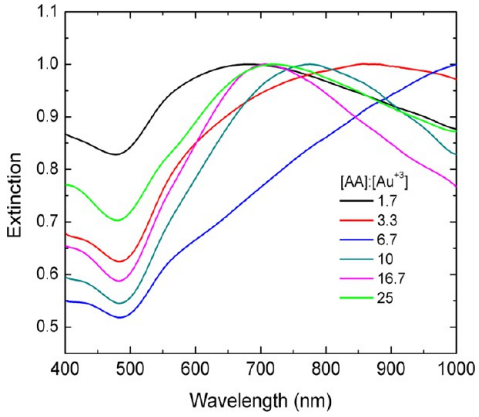

Figure 2. Effect of [AA]:[Au^{3+}] molar ratio on normalized UV−vis extinction spectra of BGNs. Volumes of Au growth solution and NP-seed were kept constant at 2.5 and 0.5 mL, respectively. The AA solution concentration was 0.5 M.

branched nanoshell growth by using a growth solution exclusively containing $HAuCl_4$, K_2CO_3 and AA. In this way, avoidance of CTAB eliminates the inherent disadvantages of its use in the synthetic process such as difficulty of clearance and potential toxicity in biomedical applications.[32,33] The reaction of $HAuCl_4$ and AA has been previously used to grow dendritic patches onto polystyrene nanospheres by exploiting the conformal surface growth of Au onto the polymeric NP surface regulated by AA surface adsorption,[37] or to obtain flower-like gold NPs by using chitosan as a stabilizing agent.[38] Silver−polymer composites were also grown using PLGA NPs to electrostatically attach silver ions and subsequently photo-reduced; capping agents such as poly(vinyl alcohol) (PVA) or sodium citrate were added prior the addition of the strong reducing agent (AA) to complete the reduction reaction.[39] However, in contrast to the methodology developed here, in the latter approach, the addition of the capping agents was key to attain the star-like structure; in its absence, only spheroidal-like particles were obtained. Hence, to the best of our knowledge, this is the first work in which the present synthetic approach is used to obtain branched gold nanoshells.

As with most anisotropic particles, the growth of the gold-branched shells on top of chitosan/F127-functionalized PLGA NPs is a seed-mediated process. In a typical synthesis (see Scheme 1), Au seeds with a diameter of ca. 3 nm were prepared by a fast reduction with sodium borohydride in the presence of sodium citrate as a capping agent (Figure S1a, Supporting Information).[18] Then, these seeds were electrostatically bound to chitosan-F127 stabilized PLGA NPs (Figure S1b, Supporting Information) (ca. 125 nm in diameter as measured by DLS and net surface charge of +15 ± 6 mV) obtained by a nanoprecipitation method in order to promote the heterogeneous nucleation onto the bound Au seeds.

To grow the branched gold nanoshells, the seed-decorated polymeric PLGA NPs were placed into a growth solution containing $HAuCl_4$ and K_2CO_3. Because of the pH-dependent weak reducing activity of AA, with values of −0.127 and −0.34 V for pH values of 4.0 and 7.0, respectively,[40] this molecule could only reduce Au salt in the presence of previously formed Au seeds (with an standard reduction potential E^0 = 1.002 V), but not isolated Au^I to Au^0 (E^0 = −1.5 V),[41] leading to a preferential reduction of Au salt on the seed surfaces. This should directly contribute to the formation of branches on the seed-decorated PLGA NPs used as nanotemplates presumably because of the slow and directional diffusion of gold precursors to the NP-attached seeds which, in the present case, is not regulated by the presence of halide ions as reported in previous works.[34] TEM images (Figure 1) revealed that synthesized BGNS were covered with branches in high yield, and the final product was free of small particles and other nanostructures. The branches formed were stable, with an average diameter and length of 14.4 ± 4.7 and 37.5 ± 7.0 nm, respectively, and hardly changed after several months of storage at room temperature under common laboratory conditions. Resulting branched Au nanoshells prepared by this process possess the advantages of

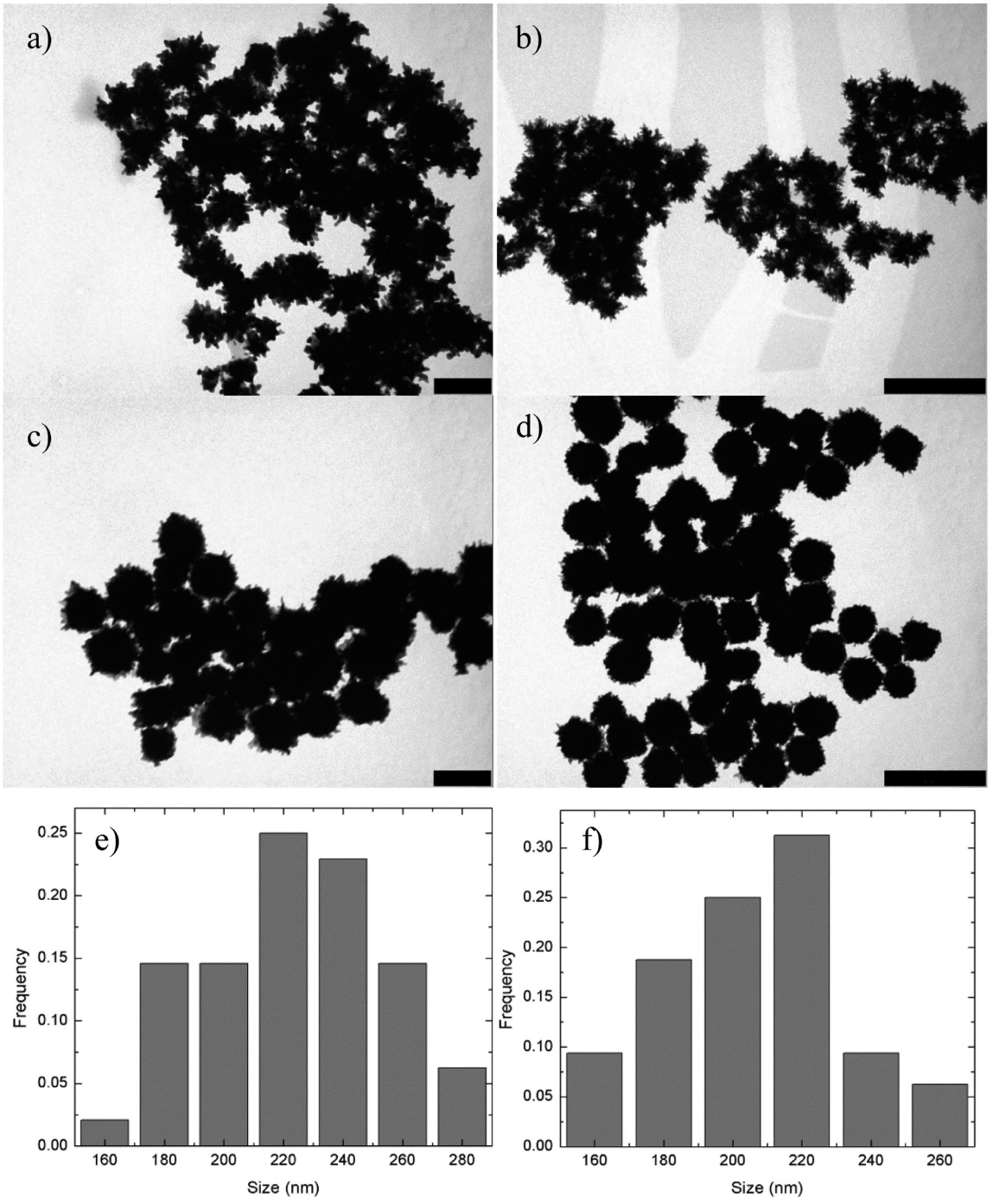

Figure 3. TEM images showing the effect of [AA] on NP size and structure. Added AA volumes (0.5 M) were (a) 10 μL, (b) 20 μL, (c) 50 μL and (d) 75 μL, corresponding to [AA]:[Au^{3+}] molar ratios of 3.3, 6.7, 16.7 and 25, respectively. Au growth solution and NP-seed volumes were kept constant at 2.5 and 0.5 mL, respectively. (e) Size distribution of BGNS observed in panel a. (f) Size distribution of BGNS observed in panel d. Scale is 200 nm in panels a and c, and 500 nm in panels b and d.

being quickly and easily obtained, enabling the control of their morphology without using toxic materials.

In this synthetic procedure chitosan plays an important role. Chitosan is a relatively stiff polymer with a large persistence length, causing the polymer chain conformation to resemble an open three-dimensional scaffold. First, chitosan chains can contribute as a reducing agent in the redox reaction of $HAuCl_4$[42,43] thanks to the high affinity of amine groups to Au, possibly acting as nucleation sites. However, in the presence of chitosan solely, 1 day is needed at least to produce a partial roughened gold coverage around the polymeric NPs, with an extinction peak centered at ca. 570 nm typical of aggregated Au NPs (Figure S2, Supporting Information). The full metal coverage of the polymeric core is not achieved, confirming that the biopolymer does not act as a strong reducing agent. The electrostatic interactions between chitosan's amine groups and primary added Au seeds and the scrolling and protrusion capacity of vicinal chitosan chains can also triggered for additional agglomeration and growth coalescence of primary seeds, which may act as secondary nuclei to give larger crystals

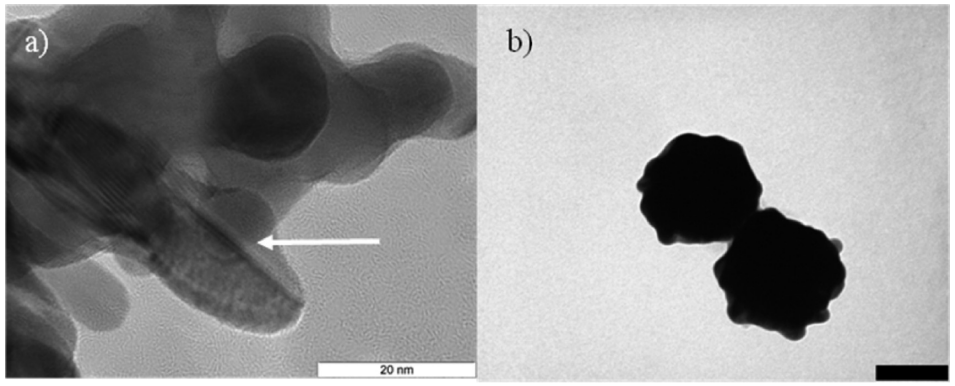

Figure 4. (a) TEM image showing the presence of twinning in branches (see arrow); (b) TEM image of nanoshells grown in the absence of chitosan, in which only small protuberances appeared. Scale bar is 100 nm.

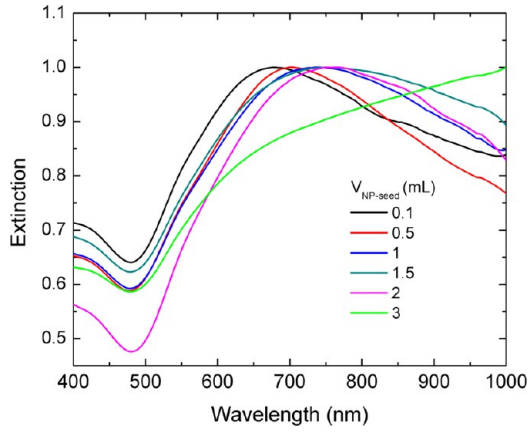

Figure 5. Effect of NP-seed on the UV–vis absorption spectra of BGNS. Volumes of Au growth solution and AA were kept constant at 2.5 mL and 50 μL, respectively ([AA]:[Au^{3+}] = 16.7). As the number of NP-seed increases, the plasmon band maximum red-shifts.

configuring the nanoshell spikes; that is, chitosan chains can also act as a structure-directing agent supporting the growth of anisotropic gold shells.[44,45] TEM and HR-TEM images confirm this point (Figure S2b,c, Supporting Information), where some agglomerates of small particles can be observed. The HR-TEM image exhibited regions of varying contrast much different from the uniformly dark particles of spherical Au nanocrystals. Also, the flat nature of these nanocrystals can be deduced by the presence of Moiré patterns arising from the presence of two superimposed, different crystal lattices.[46]

It is well-known that the plasmon peak position of smooth shells can be readily controlled by changing the ratio between the core diameter and shell thickness, and that the increased core/shell ratio results in strong red shifts of the nanoshell's plasmon band.[30] However, very large cores are often not desirable, as they significantly increase the overall particle diameter, and the preparation of very thin uniform shells can be synthetically challenging. Hence, by coupling a shell with branches one can readily tune the plasmon band over a wide wavelength range without significantly changing the nanoshell size (or the amount of gold). Trying to decipher the mechanism/s involved in their formation, we here considered the effect of the variation of different factors involved in the synthesis of these spiky gold nanoshells in order to test their influence on the reaction kinetics and on the size, shape and optical properties of the resulting particles.

3.1. Effect of Ascorbic Acid. Experimentally, the influence of AA concentration and, hence, of changes in the [AA]:[Au^{3+}] ratio on the structure and properties of BGNS was studied. As already well-known, the reduction of the auric ion by AA is stoichiometric at a molar ratio of ascorbic acid to gold (AA:Au^{3+}) of 1.5.[47] All present experiments were performed at an AA:Au^{3+} ratio above 1.7 so it is clear that the branched morphology results in the presence of an excess of AA. The increase of ascorbate ions from 0.0025 to 0.0375 mmol (corresponding to volume additions from 5 to 75 μL of a 0.5 M AA solution) led to a rapid change in solution color from colorless to blue-greenish in few seconds, indicating the main role of AA as a reducing agent.

The observed widespread heterogeneous nucleation may result from the fact that both the gold precursor, $[Au(OH)_xCl_{4-x}]^-$ and AA are expected to adsorb onto the seed-decorated core polymeric particles, further raising the probability of nucleation on the surface of NPs. AA might also bind to the chitosan chains favoring the surface reduction of Au ions in the closest vicinity of electrostatically attached gold seeds along the biopolymer chains, which would facilitate the anisotropic shell morphology. The observed changes in solution color would correspond to variations in the position of the wide plasmon absorption band of Au nanoshells spreading over ca. 500–1000 nm, as well as in the NP size and shape. In particular, the plasmon extinction peak first red-shifted from ca. 680 nm to more than 1000 nm for [AA]:[Au^{3+}] molar ratios ranging from 1.7 to 6.7, respectively, typical of the emergence and growth of multiple spikes onto their surfaces and further size increase of nanoshells (Figure 2a). TEM images showed that the products of such reactions exhibited branched structures, with the number and length of branches increasing as the AA concentration does within this concentration range (Figure 3a,b,e).

Conversely, upon addition of larger amounts of AA ([AA]:[Au^{3+}] ratios from 10 to 25), a blue shift of the plasmon peak is observed as a consequence of the progressive formation of more spheroidal and less roughened nanoshells, with an apparent growth of the nanoshell core and the reduction in the number and protrusion of spikes (Figure 3c,d,f).

The whole nanoshell diameter slightly decreased from 210 to 190 nm, as previously observed in the formation of pure gold star-shaped NPs in aqueous solution.[48] The apparent protrusion of these gold structures demonstrates that they were unlikely formed in the bulk and subsequently attached to the core-PLGA nanospheres by heterocoagulation but they

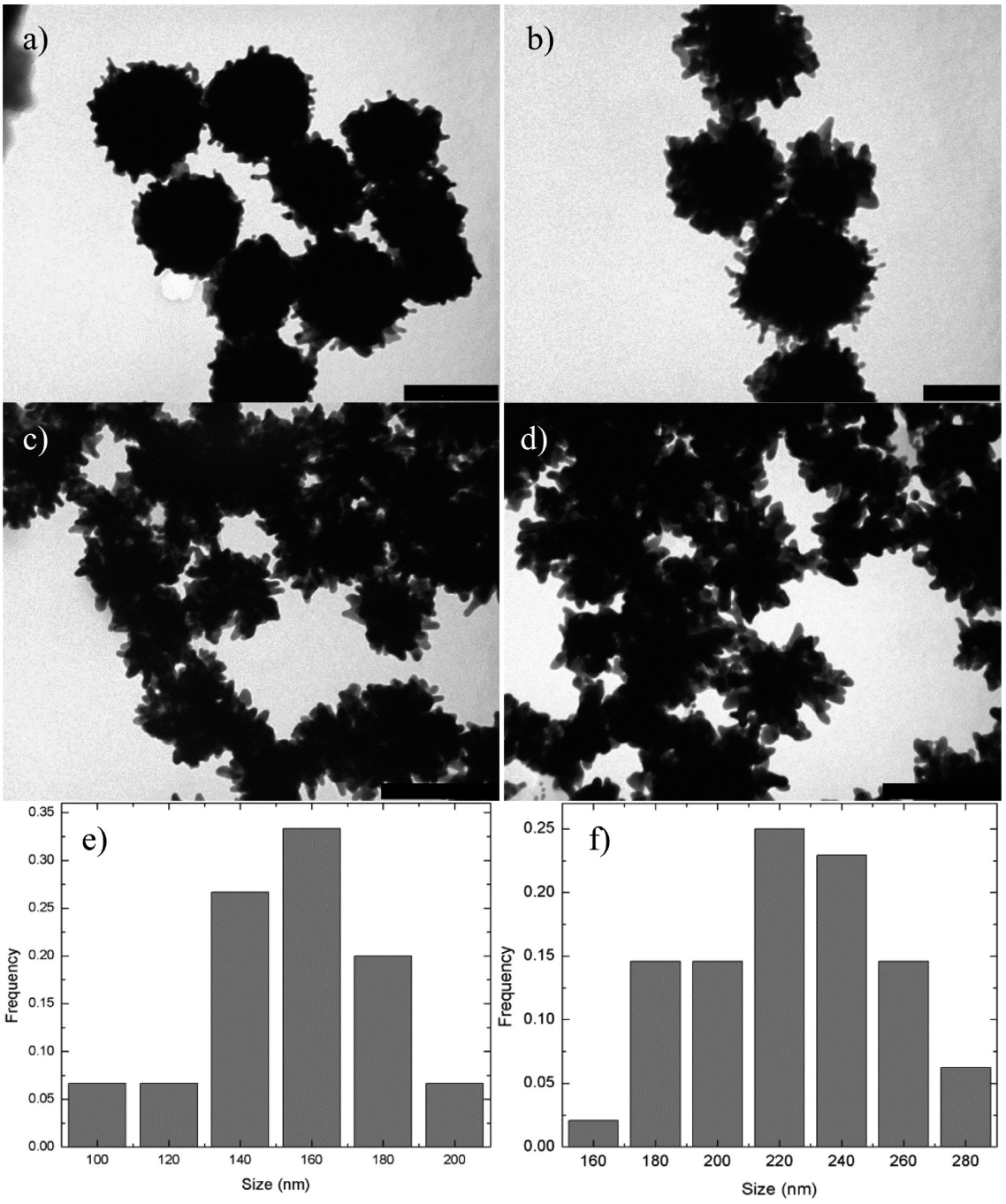

Figure 6. TEM images of BGNS showing the effect of added NP-seeds. Added volumes were (a) 0.5 mL, (b) 1 mL, (c) 2 mL and (d) 3 mL. The AA and Au growth solution molar ratio was kept constant at [AA]:[Au^{3+}] = 16.7. (e) Size distribution of BGNS observed in panel a. (f) Size distribution of BGNS observed in panel d. Scale bars are 100 nm in panels a and b, and 200 nm in panels c and d).

have been, in fact, heterogeneously nucleated and grown in all accessible dimensions (laterally as well as toward the bulk solvent). Hence, the obvious variation of nanoshell size and morphology by controlling the AA concentration clearly involved that the supply of Au^0 in the reaction system was a key for generating branched nanoshells. In this regard, it is necessary to bear in mind, on one hand, that the nature of gold reduction strongly depends on the dissociation degree of the AA molecule. As indicated in Figure S3 (Supporting Information), the pH of the reduction reactions carried out for the analyzed [AA]:[Au^{3+}] ratios varied between 2.98 (for [AA]:[Au^{3+}] = 25) and 7.15 (for [AA]:[Au^{3+}] = 1.7). With dissociation constants $pK_{a,1}$ = 4.17 and $pK_{a,2}$ = 11.58 it is, therefore, expected that mainly the nondissociated (H_2Asc) and singly deprotonated ($HAsc^-$) forms of AA participate in the gold reduction reaction. As has been previously noted, the reducing strength of ascorbic acid increases with pH, i.e., with the prevalence of the $HAsc^-$ form.[49] As observed by analyzing the reaction kinetics through spectrophotometry (see below), it can be deduced that even at low AA concentrations, the transformation of Au^I to Au^0 was sufficiently fast to induce a branched full coverage of the nanoshell surfaces, being the $HAsc^-$ form of AA the main reducing species. We then tried to isolate the effect of solution pH and, thus, on metal shell

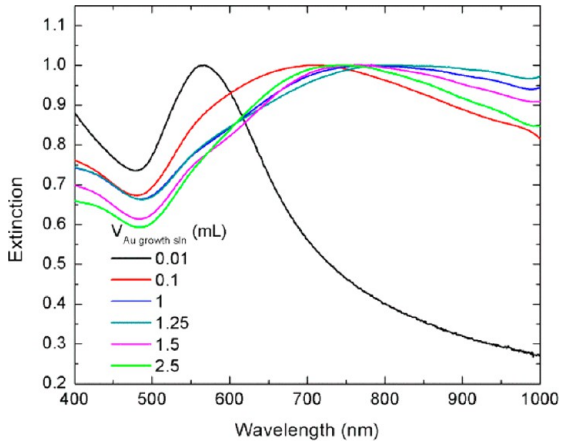

Figure 7. Effect of Au^{3+} growth solution volume on UV−vis absorption spectra of BGNS. Volumes of AA and NP-seed were kept constant at 50 μL (0.5 M) and 1 mL, respectively.

growth, by keeping constant the solution pH while adding different amounts of AA. If the pH of the reaction mixture was maintained at 4.0, it could be observed that even at low added AA concentrations, a relatively smooth gold coverage was obtained in contrast to the more branched structures observed when added the same [AA] concentration without pH control, that is, at the natural pH of the reaction solution (ca. 6.4) as a consequence of the lower reactivity of AA under acidic conditions. Conversely, if the solution pH was kept at 7.0, branched shells were obtained even at $[AA]:[Au^{3+}]$ ratios >16.7 in contrast to much more smoother shells under the natural pH of the reaction solution (ca. 3.5). At larger values, smoother shells were again obtained (Figure S4, Supporting Information). Hence, these results additionally confirm the former statements about the role played by the activity of the reducing species of AA. However, changes in reactivity of $[Au(OH)_xCl_{4-x}]^-$ species with pH (that is, with added AA) may also play a role. In this regard, Phothammachai and White have already reported that the pH of the gold plating solution was crucial for the growth of gold crystals on the surface of silica nanoparticles, suggesting the different reactivity of gold ions complex $[Au(OH)_xCl_{4-x}]^-$ would influence the formation of Au nanocrystals.[50] Also, Au−Cl complexes formed by the presence of important amounts of Cl^- and H^+ ions under acidic conditions served as transport species for Ortwald ripening on the Au layer favoring the formation of smoother gold coatings, whereas at more basic pH, the formation of less Au−Cl complexes due to the competition of OH^- with Cl^- ions in solution involved more rough surfaces as a consequence of the restriction of movement of Au atoms on the shell surface.[51]

On the other hand, the concentration-dependent facet selectivity of Au^0 onto the seed surfaces might favored the preferential growth along certain crystalline faces of the initial nuclei distributed along the extended and protruded chitosan chains (polycrystalline citrate−Au seeds), in particular, along existent twin boundaries in a kinetically controlled process as occurred for pod and star-shaped single NPs[45,47] (Figure 4a).

However, we think that the branched shell formation is largely conditioned by the presence and the ionization and conformation state of chitosan chains, which act as nucleation centers and structure directing agents. In this regard, when chitosan is absent in the reaction solution (for example, when substituted by cysteamine molecules covalently attached to PLGA carboxyl groups with EDC/sulfo-NHS), only slightly roughened nanoshell surfaces were obtained (Figure 4b). Because the pK_a of chitosan is ca. 6.5, at relatively low added AA concentrations ($[AA]:[Au^{3+}] < 6.7$), the extent of protonation of their amine groups will be largely decreased, consequently reducing to a great extent the attachment of seeds/gold ions to the polymer chains, which allows a localized nucleation and crystal growth in certain orientations leading to the anisotropic structures. On the other hand, when the added AA concentration is larger ($[AA]:[Au^{3+}] > 6.7$) an additional pH decrease takes place, being the nondissociated form of AA, H_2Asc, the main reducing species. The lowering of solution pH would lead to enhanced electrostatic interactions between positively charged chitosan chains and negatively charged gold ions ($HAuCl_4^-$) and seeds. Regardless, H_2Asc possess lower reducing activity, the combination of a large reductant excess concentration and a relatively large seed attachment onto chitosan chains would favor a more uniform metal ion deposition. Also, the AA excess might be also uniformly adsorbed on the surface of nanoshells by means of strong N−H···O−C hydrogen bonding between the amine groups of chitosan chains and the vinylogous carboxylate group of AA,[52] additionally favoring a more uniform shell growth as observed. This would highlight the multifunctional role of AA, acting as both as a reducing agent and as a stabilizer, being this effect especially relevant at high $[AA]:[Au^{3+}]$ ratios ($[AA]:[Au^{3+}] > 10$).

Hence, the previous experimental data demonstrated the possibility to tune the morphology of as-prepared nanoshells by altering, at least partially, the reduction rate of Au^I to Au^0 and/or the solution pH. Because the amount of seeds was fixed to 0.5 mL, the enhanced Au^0 concentration provided by excess of reductant, in turn, increased the Au^0/seed ratio, which represented the reactivity of gold ions. This led us to investigate the influence of other experimental variables that could improve the Au^0/seed ratio, which also allowed for tailoring the properties of the present BGNS.

3.2. Influence of NP-Seed Precursor. The influence of NP-seed concentration on the properties of as-prepared BGNS was also studied. As the amount of NP-seed increased by addition of 0.1 to 3 mL of NP-seed stock solution (with the $[AA]:[Au^{3+}]$ ratio fixed at 16.7), a progressive red shift of the wide plasmon absorption band maximum from 672 nm to >1000 nm with no signs of particle aggregation was observed (Figure 5).

Under TEM, complete nanoshell gold coverage was observed accomponied with increases in the size, number and length of the branches as the NP-seed concentration increases (Figure 6). Obviously, the addition of more seed-decorated polymeric NPs led to lower Au^0/seed ratios providing less Au^0 to supply the growth on each NP. A lower Au^0/NP seed ratio then facilitated a branched growth rather than an isotropic one, which also relied on the AA concentration as commented previously.

A control experiment indicated that at a relatively low added AA concentrations (for example, after the addition of 10 μL of a 0.25 M AA solution), the as-prepared nanoshells were even more branched in spite of NP sizes became larger with the increase of added NP-seeds (Figure S5, Supporting Information). As mentioned previously, regardless, a relatively fast reduction of Au^I to Au^0 was achievable even at low AA concentrations, which led to a relatively high reactivity of gold ions; lower Au^0/NP-seed proportions seem to favor the

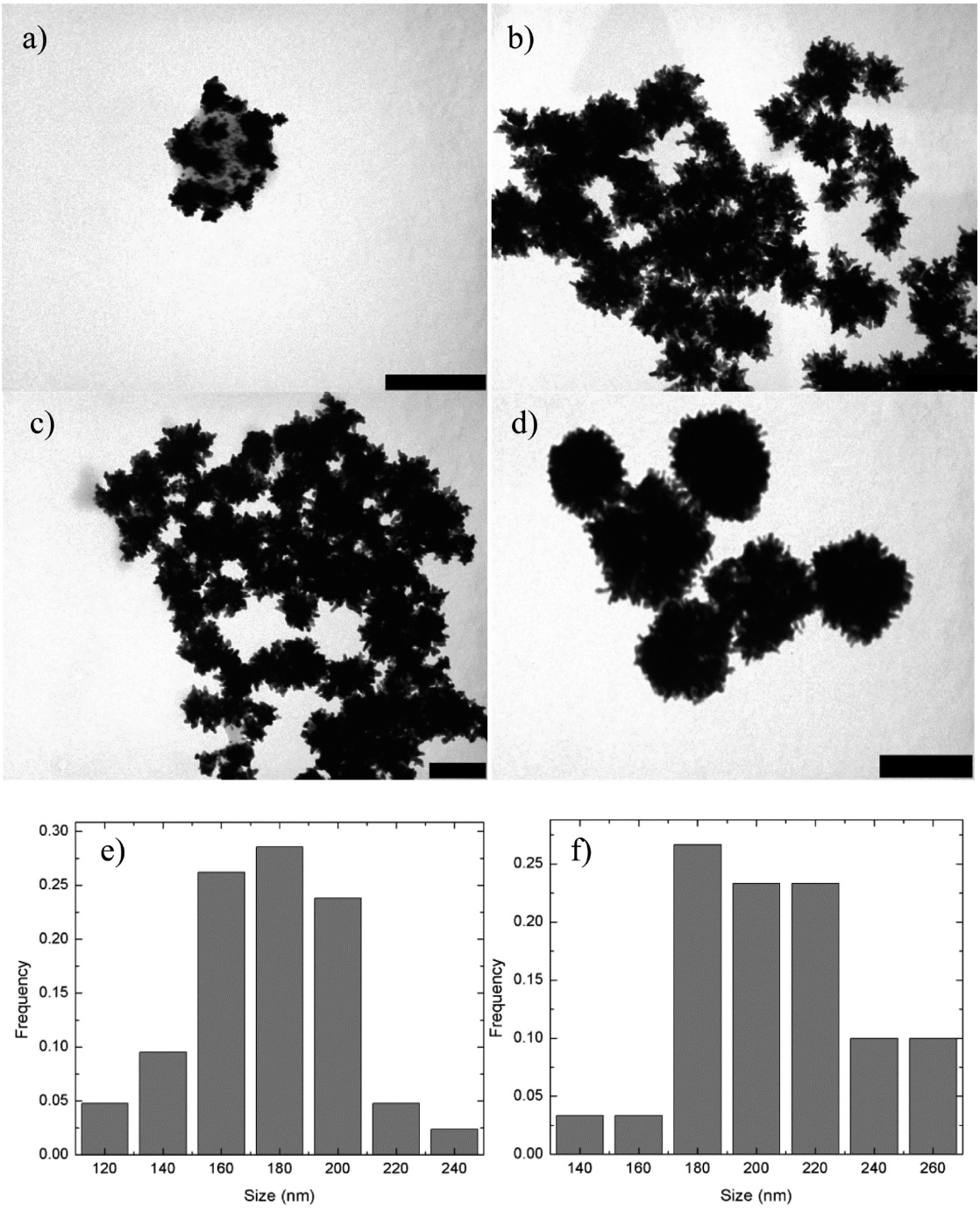

Figure 8. TEM images showing the effect of Au growth solution concentration. Added volumes of Au growth solution were (a) 0.01 mL, (b) 0.1 mL, (c) 1.25 mL and (d) 2.5 mL. AA and NP-seed volumes were kept constant at 50 μL (0.5 mM) and 1 mL, respectively. (e) Size distribution of BGNS observed in panel b. (f) Size distribution of BGNS observed in panel d. Scale bars are 200 nm.

deposition of Au on more energetically favorable directions, resulting in the anisotropic growth of the agglomerated nanocrystals around the chitosan chains.

3.3. Influence of Au Growth Solution. Another factor that changes the plasmonic properties and structure of the BGNS was the variation of $HAuCl_4$ growth solution concentration. As shown in Figure 7, increases of added gold salt at low concentrations (<0.6 μmol) led to a red shift of the BGNS plasmon absorption band from 545 to 820 nm associated with the progressive formation of a full metal layer and an increase in the number and length of spikes on the nanoshell surfaces, with whole NP sizes of ca. 188 ± 15 nm. At larger added Au^{3+} concentrations (0.75−1.5 μmol), increases of both the nanoshell core sizes and of spike widths were observed, in agreement with previous observations in section 3.2 at similar Au^0/NP-seed ratios (see Figure 6b). Thus, the shell thickness was increased, which agreed with the blue shift of the nanoshell's plasmon band from 820 to 740 nm as a consequence of the spike overlap and reduced surface roughness (Figure 8).[30]

Hence, the increase of $HAuCl_4$ at fixed AA and seed concentrations promoted the reduction of Au^{3+} to Au^+ and,

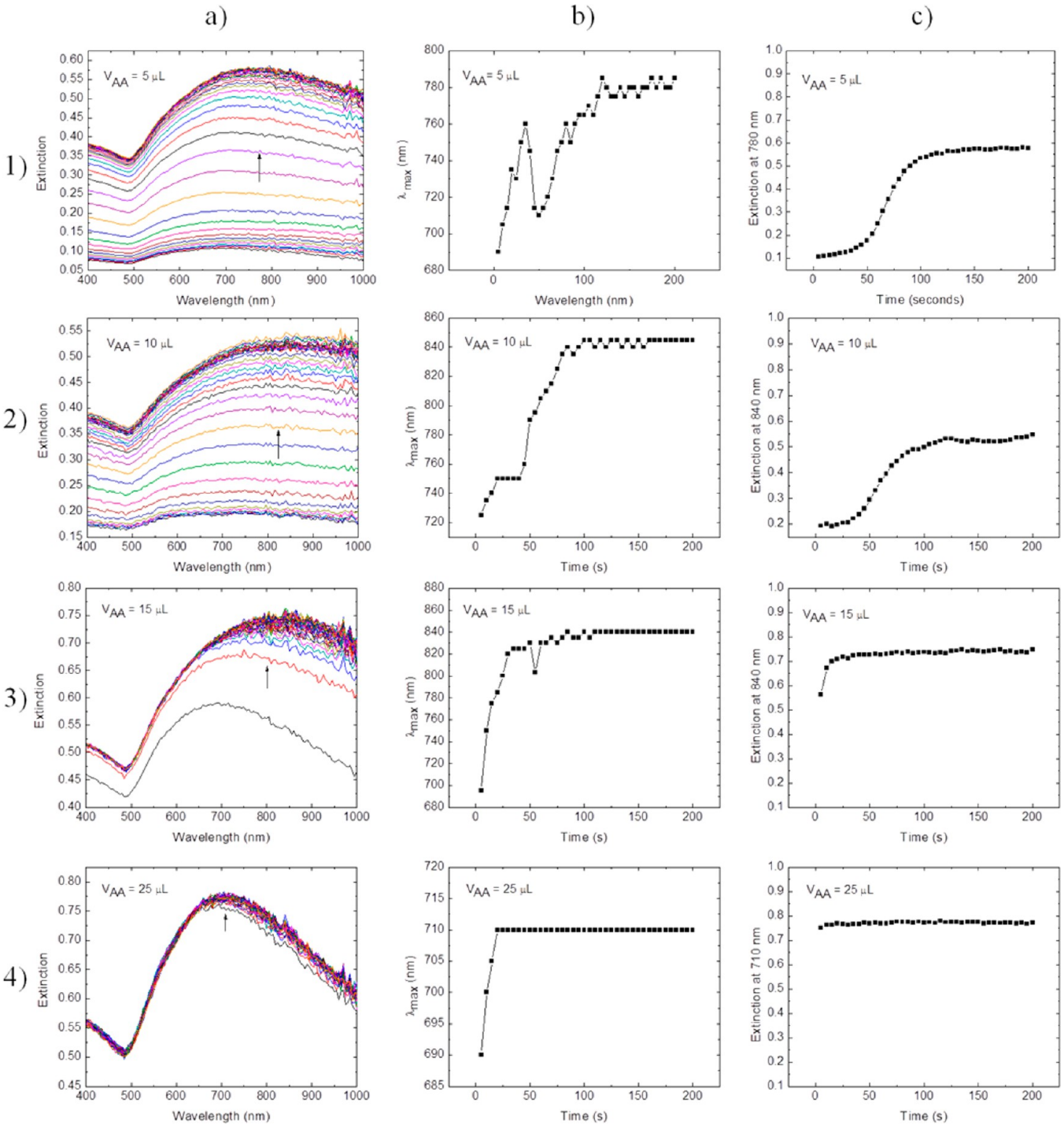

Figure 9. (a) Time evolution of UV−vis absorption spectra upon addition of different volumes of AA. Au growth solution and NP-seed were kept constant at 2.5 and 0.5 mL, respectively. (b) Time evolution of the plasmon peak wavelength position (λ_{max}). (c) Time evolution of extinction intensity at λ_{max}.

subsequently, a reduction of Au^+ to Au^0, which enhances the reactivity of gold ions. Under these conditions (relatively high concentrations of AA and NP-seeds), the formation of branched structures was first favored at low gold concentrations (hence involving lower Au^0/NP seed ratios than those analyzed in section 3.2) followed by an increase in size of the nanoshells, i.e., the shell thickness, apparently by reducing the branch lengths as a result of a much more uniform meatal coating.

3.4. Reaction Kinetics. The formation of branched-shell NPs was facilitated by a large gold reactivity under certain conditions, which was deduced as a kinetic-favored process, as previously mentioned, because branching occurs regardless of the growth solution/NP-seed ratio but being dependent on the AA concentration and solution pH. We failed to catch in most of the conditions the whole extension of the time-dependent kinetics of branched-shell growth provided that they are almost instantaneously formed after the addition of AA.

When possible, the spectra measured in situ during the shell growth denote, on one hand, gradual red shifts of the plasmon bands into the NIR region and, on the other, increases in light

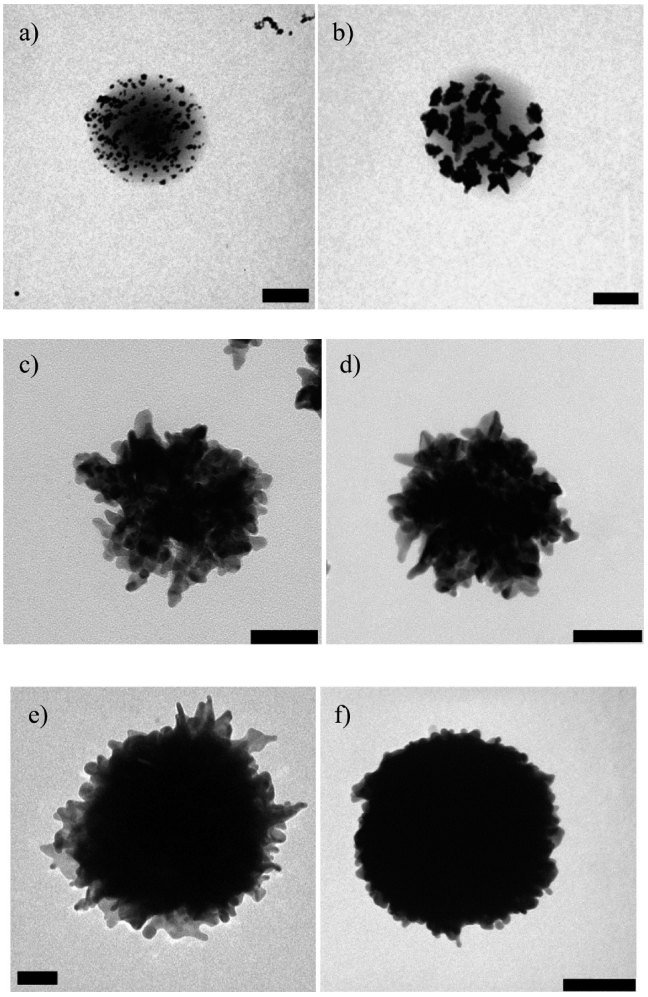

Figure 10. TEM images of BGNS growth. Reactants volumes were 2.5 mL of Au growth solution, 0.5 mL of NP-seed and 30 μL of AA (0.5 M), respectively. Aliquots (10 μL) of the reaction mixture were taken at (a) 0, (b) 5, (c) 60, (d) 120, (e) 180 s and (f) 8 min. Scale bars are 50 nm in panels a, b and e, and 100 nm in panels c, d and f.

extinction with reaction time until reaching a plateau value as a consequence of the progressive increase in shell thickness and the number and length of spikes (Figure 9). In particular, as the added AA concentration increases, the plasmon band additionally red-shifts during the metal shell growth and the reaction kinetics became faster. Above 20 μL of added AA (0.5 M), the reduction reaction takes place instantaneously but a red shift of the plasmon band with time can be also noted; however, the absolute final position of the maximum blue-shifts due to the observed changes in structure of the resulting nanoshells, as mentioned previously in section 3.1. For example, we could observe that upon injection of 5 μL of a 0.50 M AA solution, the extinction reached its maximum within ca. 120 s (Figure 9, row 1) and the plasmon peak is red-shifted ca. 100 nm from the first time point measured (at 5 s). However, TEM images obtained at short reaction times under the former reaction conditions allowed to observe that the branch formation onto the electrostatically attached seeds might already occur at the earliest stages of the gold nanolayer formation, that is, when this nanoshell is not fully developed (Figure 10a,b), in contrast to previous observations by Wei et al.[53] and Park et al.[33] where a very fast isotropic growth of gold islands takes first place followed by the anisotropic growth of sharp branches onto these islands. As the reaction carried on, the polymeric NPs were fully covered with a gold shell which became thicker and more branched after completion of the reduction reaction due to the progressive depletion of the gold ions, which deposited on more energetically preferred directions (Figure 10c,d).[52] This fact would be additionally facilitated through the role played by chitosan as agglomerating and directing agent of crystal seeds in their vicinity to give intermediate particles probably with crystal plane defects, which may additionally act as additional nucleation growth centers for branch formation.[55]

It is worth mentioning that a slight blue shift of the plasmon absorption band of ca. 30 nm is observed when the nanoshell growth time is maintained from 3 to 8 min, followed by a constant value if additionally prolonged (Figure S6, Supporting Information). Within this time period, the nanoshell morphology was slightly tuned from spiky to smoother gold nanoshells (Figure 10f). These results would be consistent with a kinetic-favored growth mechanism for the anisotropic gold nanoshells.[56] Namely, the kinetic-favored formation of the branched shells should be thermodynamically unstable and tended to transform to isotropic shells.[57] Consequently, it seems that after ca. 8 min, a thermodynamic equilibrium of the NP surfaces structure was built up through the reorganization of their sizes of surface atoms which, in turn, suppressed the additional transformation of the NP morphology and, thereby, the blue shift of absorption spectra.

The existence of highly active facets was confirmed by powder XRD and HRTEM observation of spiky nanoshells (Figure 11). XRD indicated that the lattice parameters of the spiky nanoshells fitted well to the face-centered-cubic structure of bulk gold crystal, showing reflections in the 2θ range of 25−70° indexable to the (111), (200) and (220) reflections of fcc Au (JCPDS, file no. 4-0784) (Figure 10a).[55] SAED patterns also confirmed that these branched nanoshells were crystalline and randomly oriented, confirming the diffraction peaks obtained by XRD (Figure 11b). The appearance of these peaks meant that the spiky nanoshells were polycrystalline, in particular, formed by a polycrystalline core with a number of single crystal spikes branching out from the surface. Besides, the nanoshells possessed the strongest (111) diffraction peak, indicating that the branched growth of these hybrid particles might be through the deposition of Au^0 mainly on (111) lattice planes. This consideration was further proved by HRTEM (Figure 11c). Under HRTEM, interplanar distances in elongated single branches were found to be 0.236 nm, corresponding to (111) lattice planes, whereas in some branches formed by several agglomerated crystals an interplanar spacing of 0.206 nm was also found, corresponding to (200) lattice planes. This result is reasonable because, despite that the XRD and SAED patterns show predominace of (111) lattice planes, peaks belonging to (200) and (220) crystal planes with sufficient intensity are also present. For the analyzed branches, the growth direction was vertical to the (111) plane, indicating that this plane can be a high-energy facet and allowed preferential deposition of gold ions.

The kinetics-favored profile of the spiky shell growth was further proved by a stepwise addition of AA. In general, the UV−vis spectra and, thus, the morphology of as-prepared nanoshells were partially determined by the AA amount of the primary addition, which did not relate to the total amount of AA (Figure S7a−d, Supporting Information). The nanoshell size via stepwise addition of AA was smaller than those via one-off addition (from 200 to 180 nm, Figure S7e,f, Supporting

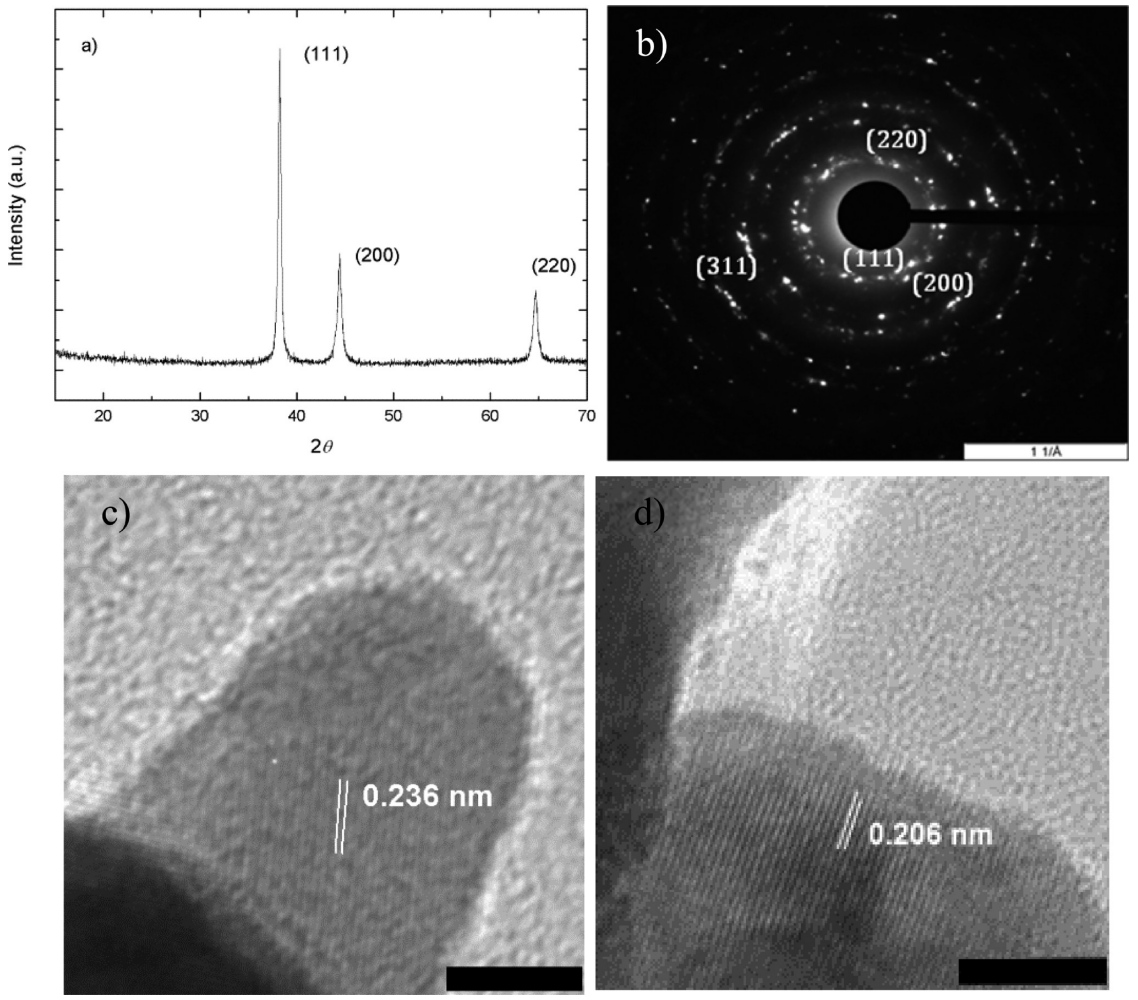

Figure 11. (a) XRD pattern and (b) SAED pattern of BGNS. (c) HRTEM of one branch with an interplanar distance of 0.236 nm corresponding to (111) lattice planes and (d) with 0.206 nm of interplanar distance corresponding to (200) lattice planes. Scale bars in panels c and d are 5 nm.

Information). This fact revealed that the formation of the branched shells was mostly favored by a sufficient initial concentration of Au^0 through AA reduction rather than its total concentration during the reaction. Interestingly, the time interval between the two injection steps also influenced the plasmon absorption band and size of the nanoshells attributed to the different face activity of gold seeds and particles during the different growth time intervals (Figure 11d), as observed in previous works.[54] Similarly, it was also found that the use of seeds stored within 1 day after preparation resulted in more branched nanoshells than that over 1 day, provided that the former possessed active facets with higher surface energy, facilitating the deposition of Au^0 along these facets and therefore, the branched growth of the shells.

3.5. In Vitro Cytotoxicity Assay. To determine the feasibility to use our BGNS for biomedical applications, we preliminarily tested the potential biocompatibility of the as-obtained BGNS by using the resazurin cell viability assay in order to establish if the BGNS synthesized through the present protocol could be potentially used in biomedical applications. Resazurin is a blue dye, itself weakly fluorescent until it is irreversibly reduced to the pink colored and highly red fluorescent resorufin. Resazurin is effectively reduced in mitochondria in the presence of diaphorase as the enzyme, and NADPH or NADH the reductant that converts resazurin to resorufin. Then, this conversion makes useful this test to analyze cell viability by assaying the cell mitochondrial activity.

Cell viability of pegylated BGNS was assayed in a HeLa cervical cancer cell line in a wide range of particle concentrations (ca. 2×10^8–2×10^{11} NP/mL). As observed in Figure 12a, the cell viability was above 90% in the whole concentration range except at the largest concentration, for which it decreases to ca. 83%. These data denote a priori a good biocompatibility of this kind of particles. To reject possible false positives and to confirm the effective incorporation of the NPs inside the cells, optical and transmission electron microscopies were performed. In this way, BGNS seem to be internalized by the cells and are present, to a large extent, in the cell cytoplasm and surrounding the cell nuclei but not inside, as observed from differential interference contrast (DIC) optical microscopy images (Figure 12b). TEM images also confirmed the internalization of the present type of particles inside the cell cytoplasm (in particular, inside intracellular vacuoles, see Figure 12c,d), probably occurring via a nonspecific endocytosis pathway.

Surface chemistry of metallic nanoparticles has a strong influence on their biocompatibility, especially when the stabilizer/directing agent is cytotoxic. For example, phosphatidylcholine-stabilized or pegylated nanorods have been found to possess much smaller or negligible toxicity as compared to

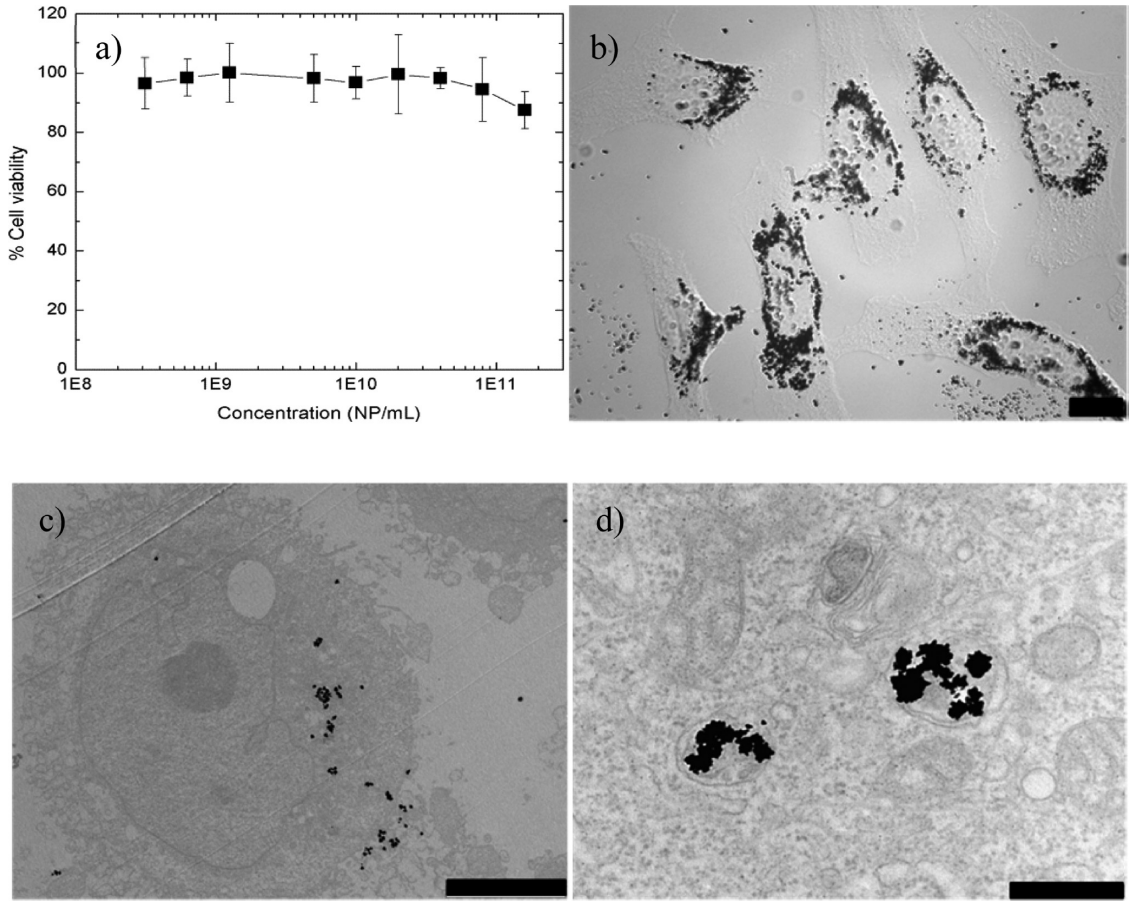

Figure 12. (a) Cell viability of HeLa cells after incubation with pegylated BGNS determined by the resazurin viability test. Cytotoxicity of BGNS was negligible in a wide concentration range (2×10^8–2×10^{11} NP/mL). (b) DIC microscopy image of HeLa cells after incubation with BGNS. (c) Internalization of BGNS into HeLa cells as visualized by TEM. (d) The formation of intracellular vacuoles suggests that BGNS are internalized via nonspecific endocystosis. Scale bars are 20 μm in panel b, 5 μm in panel c and 500 nm in panel d).

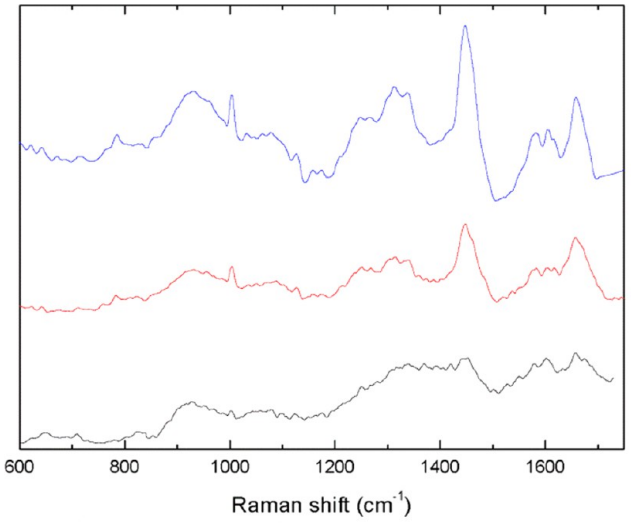

Figure 13. Averaged Raman spectra on HeLa cell without nanoshells (black) and averaged SERS spectra by excitation of smooth (red) and spiky (blue) nanoshells in different cells at approximate locations under light excitation of 785 nm.

CTAB-stabilized nanorods, as reported by Niidome et al.[58,59] To the best of our knowledge, there are no cytotoxicity results reported for CTAB-stabilized spiky gold nanoparticles to compare our results, but from reports for Au nanorods, it is reasonable to conclude that CTAB-stabilized spiky nanoshells would have much higher toxicity originated mainly from CTAB surfactant.

3.6. Intracellular Surface-Enhanced Raman Spectroscopy (SERS). Gold nanoshells have been found to be optimal substrates for SERS,[60−62] upon illumination with light of suitable wavelengths, thanks to the control of the core and shell dimensions, which enables the tunability of their plasmon resonance frequencies to enhance the inherently weak Raman signal of molecules in the vicinity of the particle surface. The presence of sharp branches acting as "hot-spots" on the nanoshell surfaces should additionally increase the Raman signal if compared to smooth nanostructures. Hence, we performed a preliminary experiment in order to verify that BGNS are more suitable to acquire SERS spectra from the intracelllular environment of living HeLa cells.

As seen previously, the present BGNS displayed localized surface plasmon centered in the NIR region, so particle excitation was performed with a 785 nm NIR laser, which have excellent transmittance through tissue. Figure 13 compares the unenhanced Raman measurements and SERS spectra enhanced by intracellular smooth and spiky Au nanoshells in HeLa grown on quartz coverslips. The spectra were taken in several living cells in approximate similar locations where nanoshells were present and averaged. Comparing the obtained spectra, we observed that some similar features are visible, such as the peak

at ca. 930 for C−C skeletal stretch in protein, ca. 1005 cm^{-1} for phenylalanine, ca. 1127 and 1175 cm^{-1} for C−N and C−C stretches in polypeptide chains, ca. 1447 cm^{-1} for chromophore aromatic ring stretches, ca. 1579 cm^{-1} for tyrosine stretching, ca. 1604 cm^{-1} for bending of phenyalanine and tyrosine, or at ca. 1658 cm^{-1} for amide I:α-helix. No clear DNA-related peaks in the SERS spectra of nanoshells are found in agreement with their cytosolic localization. In addition, it can be observed that the SERS signal from BGNS is clearly enhanced compared to that of smoother Au nanoshells, with a relative estimated SERS increment of ca. 10^3 (see the Supporting Information).[62,63] This enhancement should stem from the field concentration at the apex of the tips of the BGNS, provided that the internalization extent of both BGNS and smooth nanoshells was rather similar as confirmed by ICP-MS. Finally, it is worth mentioning that under the selected irradiation conditions, no visible signal of damage was observed in the films, indicating that NIR light can be a suitable source of light for SERS experiments on biological samples.

4. CONCLUSIONS

In summary, we have synthesized branched gold nanoshells (BGNS) with PLGA cores by means of a surfactant-less method, using a $HAuCl_4/K_2CO_3$ growth solution and concentrated ascorbic acid as the reductant. Size and structure (anisotropy) and, in consequence, the optical properties of nanostructures were tuned by modulating the synthetic conditions (feed ratios of AA and NP-seed precursor). Both chitosan and AA played an important role as coreductants and directing agents, resulting in the growth of branched structures resembling geometries found in nature, such as viruses, sea urchins or bushes. The concentration of AA was dominant to enhance the reactivity of gold ions by reduction of Au^I to Au^0 on the seed surfaces onto preferred facet via a kinetics-favored process. This process is additionally assisted by the presence of the chitosan chains and their pH solution dependence, which enables the formation of nanocrystal agglomerates, which can serve as secondary nucleation centers, and can direct the crystal growth through preferred orientations. An excessive amount of AA promotes an instant reduction of the particles, decreasing their anisotropy by the isotropic deposition of the gold ions and the adsorption of excess AA on the surface of nanoshells. Meaningfully, the as-prepared BGNS were stable in aqueous solution for several months, and were found to be internalized by cells in the cytoplasm and fully biocompatible, as deduced from a cell viability test. The hollow and branched architecture of BGNS is also advantageous because it adds another control characteristic to tune the plasmon band position to the near-infrared region of the electromagnetic spectrum, allowing their potential use as intracellular surface enhanced Raman scattering (SERS) probes. In addition, other functional materials and molecules can be incorporated into the core to fabricate multifunctional materials. In this way, these branched hollow NPs hold potential applicability as multifunctional nano-theranostic agents due to their optical properties and core-carrying capacity.

■ ASSOCIATED CONTENT

Supporting Information

TEM images of citrate-capped gold seeds and PLGA NPs; UV−vis spectrum, TEM image of NPs obtained in the absence of AA and HR-TEM of BGNS showing the Moiré patterns; TEM images of BGNS produced at different pH and AA concentration; TEM image of BGNS produced with 10 μL of 0.25 M AA; UV−vis spectra of BGNS at different reduction times; UV−vis spectra and TEM images of BGNS obtained by varying the way of adding the AA; equation to estimate the SERS enhancement. This material is available free of charge via the Internet at http://pubs.acs.org.

■ AUTHOR INFORMATION

Corresponding Authors

*S. Barbosa. E-mail: silvia.barbosa@usc.es.

* P. Taboada. E-mail: pablo.taboada@usc.es.

Present Addresses

[†]Departamento de Procesos y Bioteconología, Universidad Autónoma Metropolitana, Unidad Cuajimalpa, Vasco de Quiroga 4871, México. D. F. 05348.

[‡]3B's Research Group—Biomaterials, Biodegradables and Biomimetics, University of Minho, 4806-909 Guimarães, Portugal.

Notes

The authors declare no competing financial interest.

■ ACKNOWLEDGMENTS

The authors thank Ministerio de Economía y Competitividad (MINECO) for research project MAT 2010-17336, Xunta de Galicia for research grants CN2012/072 and EM2013-046 and fundación Ramón Arece for additional financial support. S.B. also thanks MINECO for her Ramón y Cajal fellowship. The authors also specially thank staff of Instituto de Ortopedia y Banco de tejidos Musculoesqueléticos of the Universidad de Santiago de Compostela, and especially to Maite Silva, for helpful assistance during in vitro cell experiments. A.T. and M.A.-M. thank Mexico's National Council of Science and Technology (CONACYT) for grants No. 308128 and No. 203732, respectively.

■ REFERENCES

(1) Sau, T. K.; Rogach, A. L. Nonspherical Noble Metal Nanoparticles: Colloid-Chemical Synthesis and Morphology Control. *Adv. Mater.* **2010**, *22*, 1781−1804.

(2) Zhao, P.; Li, N.; Astruc, D. State of the Art in Gold Nanoparticle Synthesis. *Coord. Chem. Rev.* **2013**, *257*, 638−665.

(3) Grzelczak, M.; Perez-Juste, J.; Mulvaney, P.; Liz-Marzan, L. M. Shape Control in Gold Nanoparticle Synthesis. *Chem. Soc. Rev.* **2008**, *37*, 1783−1791.

(4) Kelly, K. L.; Coronado, E.; Zhao, L. L.; Schatz, G. C. The Optical Properties of Metal Nanoparticles: The Influence of Size, Shape, and Dielectric Environment. *J. Phys. Chem. B* **2002**, *107*, 668−677.

(5) Guerrero-Martínez, A.; Barbosa, S.; Pastoriza-Santos, I.; Liz-Marzán, L. M. Nanostars Shine Bright for You: Colloidal Synthesis, Properties and Applications of Branched Metallic Nanoparticles. *Curr. Opin. Colloid Interface Sci.* **2011**, *16*, 118−127.

(6) Bardhan, R.; Grady, N. K.; Cole, J. R.; Joshi, A.; Halas, N. J. Fluorescence Enhancement by Au Nanostructures: Nanoshells and Nanorods. *ACS Nano* **2009**, *3*, 744−752.

(7) Link, S.; El-Sayed, M. A. Shape and Size Dependence of Radiative, Non-Radiative and Photothermal Properties of Gold Nanocrystals. *Int. Rev. Phys. Chem.* **2000**, *19*, 409−453.

(8) Jena, B. K.; Raj, C. R. Seedless, Surfactantless Room Temperature Synthesis of Single Crystalline Fluorescent Gold Nanoflowers with Pronounced SERS and Electrocatalytic Activity. *Chem. Mater.* **2008**, *20*, 3546−3548.

(9) Wang, W.; Pang, Y.; Yan, J.; Wang, G.; Suo, H.; Zhao, C.; Xing, S. Facile Synthesis of Hollow Urchin-like Gold Nanoparticles and Their Catalytic Activity. *Gold Bull.* **2012**, *45*, 91−98.

(10) Loo, C.; Hirsch, L.; Lee, M.-H.; Chang, E.; West, J.; Halas, N.; Drezek, R. Gold Nanoshell Bioconjugates for Molecular Imaging in Living Cells. *Opt. Lett.* **2005**, *30*, 1012−1014.
(11) Khanadeev, V. A.; Khlebtsov, B. N.; Staroverov, S. A.; Vidyasheva, I. V.; Skaptsov, A. A.; Ileneva, E. S.; Bogatyrev, V. A.; Dykman, L. A.; Khlebtsov, N. G. Quantitative Cell Bioimaging Using Gold-Nanoshell Conjugates and Phage Antibodies. *J. Biophotonics* **2011**, *4*, 74−83.
(12) Stewart, M. E.; Anderton, C. R.; Thompson, L. B.; Maria, J.; Gray, S. K.; Rogers, J. A.; Nuzzo, R. G. Nanostructured Plasmonic Sensors. *Chem. Rev.* **2008**, *108*, 494−521.
(13) Carregal-Romero, S.; Ochs, M.; Rivera-Gil, P.; Ganas, C.; Pavlov, A. M.; Sukhorukov, G. B.; Parak, W. J. NIR-Light Triggered Delivery of Macromolecules into the Cytosol. *J. Controlled Release* **2012**, *159*, 120−127.
(14) Braun, G. B.; Pallaoro, A.; Wu, G.; Missirlis, D.; Zasadzinski, J. A.; Tirrell, M.; Reich, N. O. Laser-Activated Gene Silencing via Gold Nanoshell−siRNA Conjugates. *ACS Nano* **2009**, *3*, 2007−2015.
(15) Hu, M.; Chen, J.; Li, Z.-Y.; Au, L.; Hartland, G. V.; Li, X.; Marquez, M.; Xia, Y. Gold Nanostructures: Engineering Their Plasmonic Properties for Biomedical Applications. *Chem. Soc. Rev.* **2006**, *35*, 1084−1094.
(16) Turkevich, J.; Stevenson, P. C.; Hillier, J. A Study of the Nucleation and Growth Processes in the Synthesis of Colloidal Gold. *Discuss. Faraday Soc.* **1951**, *11*, 55−75.
(17) Bastús, N. G.; Comenge, J.; Puntes, V. C. Kinetically Controlled Seeded Growth Synthesis of Citrate-Stabilized Gold Nanoparticles of up to 200 nm: Size Focusing versus Ostwald Ripening. *Langmuir* **2011**, *27*, 11098−11105.
(18) Jana, N. R.; Gearheart, L.; Murphy, C. J. Wet Chemical Synthesis of High Aspect Ratio Cylindrical Gold Nanorods. *J. Phys. Chem. B* **2001**, *105*, 4065−4067.
(19) Nikoobakht, B.; El-Sayed, M. A. Preparation and Growth Mechanism of Gold Nanorods (NRs) Using Seed-Mediated Growth Method. *Chem. Mater.* **2003**, *15*, 1957−1962.
(20) Millstone, J. E.; Métraux, G. S.; Mirkin, C. A. Controlling the Edge Length of Gold Nanoprisms via a Seed-Mediated Approach. *Adv. Funct. Mater.* **2006**, *16*, 1209−1214.
(21) Wang, Y.; Black, K. C. L.; Luehmann, H.; Li, W.; Zhang, Y.; Cai, X.; Wan, D.; Liu, S.-Y.; Li, M.; Kim, P.; Li, Z.-Y.; Wang, L. V.; Liu, Y.; Xia, Y. Comparison Study of Gold Nanohexapods, Nanorods, and Nanocages for Photothermal Cancer Treatment. *ACS Nano* **2013**, *7*, 2068−2077.
(22) Pelaz, B.; Grazu, V.; Ibarra, A.; Magen, C.; del Pino, P.; de la Fuente, J. M. Tailoring the Synthesis and Heating Ability of Gold Nanoprisms for Bioapplications. *Langmuir* **2012**, *28*, 8965−8970.
(23) Averitt, R. D.; Sarkar, D.; Halas, N. J. Plasmon Resonance Shifts of Au-Coated Au_2S Nanoshells: Insight into Multicomponent Nanoparticle Growth. *Phys. Rev. Lett.* **1997**, *78*, 4217−4220.
(24) You, J.; Zhang, G.; Li, C. Exceptionally High Payload of Doxorubicin in Hollow Gold Nanospheres for Near-Infrared Light-Triggered Drug Release. *ACS Nano* **2010**, *4*, 1033−1041.
(25) Kawamura, G.; Yang, Y.; Fukuda, K.; Nogami, M. Shape Control Synthesis of Multi-Branched Gold Nanoparticles. *Mater. Chem. Phys.* **2009**, *115*, 229−234.
(26) Yang, J.; Lee, J.; Kang, J.; Oh, S. J.; Ko, H.-J.; Son, J.-H.; Lee, K.; Suh, J.-S.; Huh, Y.-M.; Haam, S. Smart Drug-Loaded Polymer Gold Nanoshells for Systemic and Localized Therapy of Human Epithelial Cancer. *Adv. Mater.* **2009**, *21*, 4339−4342.
(27) Bardhan, R.; Chen, W.; Perez-Torres, C.; Bartels, M.; Huschka, R. M.; Zhao, L. L.; Morosan, E.; Pautler, R. G.; Joshi, A.; Halas, N. J. Nanoshells with Targeted Simultaneous Enhancement of Magnetic and Optical Imaging and Photothermal Therapeutic Response. *Adv. Funct. Mater.* **2009**, *19*, 3901−3909.
(28) Hao, F.; Nehl, C. L.; Hafner, J. H.; Nordlander, P. Plasmon Resonances of a Gold Nanostar. *Nano Lett.* **2007**, *7*, 729−732.
(29) Baffou, G.; Quidant, R.; Girard, C. Heat Generation in Plasmonic Nanostructures: Influence of Morphology. *Appl. Phys. Lett.* **2009**, *94*, 153109/1−153109/3.
(30) Wang, H.; Goodrich, G. P.; Tam, F.; Oubre, C.; Nordlander, P.; Halas, N. J. Controlled Texturing Modifies the Surface Topography and Plasmonic Properties of Au Nanoshells. *J. Phys. Chem. B* **2005**, *109*, 11083−11087.
(31) Wang, H.; Fu, K.; Drezek, R. A.; Halas, N. J. Light Scattering from Spherical Plasmonic Nanoantennas: Effects of Nanoscale Roughness. *Appl. Phys. B: Laser Opt.* **2006**, *84*, 191−195.
(32) Sanchez-Gaytan, B. L.; Swanglap, P.; Lamkin, T. J.; Hickey, R. J.; Fakhraai, Z.; Link, S.; Park, S.-J. Spiky Gold Nanoshells: Synthesis and Enhanced Scattering Properties. *J. Phys. Chem. C* **2012**, *116*, 10318−10324.
(33) Sanchez-Gaytan, B. L.; Park, S.-J. Spiky Gold Nanoshells. *Langmuir* **2010**, *26*, 19170−19174.
(34) Sanchez-Gaytan, B. L.; Qian, Z.; Hastings, S. P.; Reca, M. L.; Fakhraai, Z.; Park, S.-J. Controlling the Topography and Surface Plasmon Resonance of Gold Nanoshells by a Templated Surfactant-Assisted Seed Growth Method. *J. Phys. Chem. C* **2013**, *117*, 8916−8923.
(35) Garg, N.; Scholl, C.; Mohanty, A.; Jin, R. The Role of Bromide Ions in Seeding Growth of Au Nanorods. *Langmuir* **2010**, *26*, 10271−10276.
(36) Goia, D.; Matijević, E. Tailoring the Particle Size of Monodispersed Colloidal Gold. *Colloids Surf., A* **1999**, *146*, 139−152.
(37) Bao, H.; Bihr, T.; Smith, A.-S.; Klupp; Taylor, R. N. Facile Colloidal Coating of Polystyrene Nanospheres with Tunable Gold Dendritic Patches. *Nanoscale* **2014**, *6*, 3954−3966.
(38) Nhung, T. T.; Bu, Y.; Lee, S.-W. Facile Synthesis of Chitosan-Mediated Gold Nanoflowers as Surface-Enhanced Raman Scattering (SERS) Substrates. *J. Cryst. Growth* **2013**, *373*, 132−137.
(39) Homan, K. A.; Chen, J.; Schiano, A.; Mohamed, M.; Willets, K. A.; Murugesan, S.; Stevenson, K. J.; Emelianov, S. Silver−Polymer Composite Stars: Synthesis and Applications. *Adv. Funct. Mater.* **2011**, *21*, 1673−1680.
(40) Valenzuela, K.; Raghavan, S.; Deymier, P. A.; Hoying, J. Formation of Copper Nanowires by Electroless Deposition Using Microtubules as Templates. *J. Nanosci. Nanotechnol.* **2008**, *8*, 3416−3421.
(41) Perrault, S. D.; Chan, W. C. W. Synthesis and Surface Modification of Highly Monodispersed, Spherical Gold Nanoparticles of 50−200 nm. *J. Am. Chem. Soc.* **2009**, *131*, 17042−17043.
(42) Xu, D.; Gu, J.; Wang, W.; Yu, X.; Xi, K.; Jia, X. Development of Chitosan-coated Gold Nanoflowers as SERS-active Probes. *Nanotechnology* **2010**, *21*, 375101.
(43) Boca, S.; Rugina, D.; Pintea, A.; Barbu-Tudoran, L.; Astilean, S. Flower-Shaped Gold Nanoparticles: Synthesis, Characterization and Their Application as SERS-Active Tags Inside Living Cells. *Nanotechnology* **2011**, *22*, 055702.
(44) Wang, W.; Cui, H. Chitosan-Luminol Reduced Gold Nanoflowers: From One-Pot Synthesis to Morphology-Dependent SPR and Chemiluminescence Sensing. *J. Phys. Chem. C* **2008**, *112*, 10759−10766.
(45) Wang, W.; Yang, X.; Cui, H. Growth Mechanism of Flowerlike Gold Nanostructures: Surface Plasmon Resonance (SPR) and Resonance Rayleigh Scattering (RRS) Approaches to Growth Monitoring. *J. Phys. Chem. C* **2008**, *112*, 16348−16353.
(46) Williams, D. B.; Carter-Barry, C. *Transmission Electron Microscopy: A Textbook for Materials Science*; Springer: New York, 2009.
(47) Bode, A. M.; Cunningham, L.; Rose, R. C. Spontaneous Decay of Oxidized Ascorbic Acid (Dehydro-L-Ascorbic Acid) Evaluated by High-Pressure Liquid Chromatography. *Clin. Chem.* **1990**, *36*, 1807−1809.
(48) Sau, T. K.; Rogach, A. L.; Döblinger, M.; Feldmann, J. One-Step High-Yield Aqueous Synthesis of Size-Tunable Multispiked Gold Nanoparticles. *Small* **2011**, *7*, 2188−2194.
(49) Luty-Błocho, M.; Pacławski, K.; Wojnicki, M.; Fitzner, K. The Kinetics of Redox Reaction of Gold(III) Chloride Complex Ions with l-Ascorbic Acid. *Inorg. Chim. Acta* **2013**, *395*, 189−196.

(50) Phonthammachai, N.; White, T. J. One-Step Synthesis of Highly Dispersed Gold Nanocrystals on Silica Spheres. *Langmuir* **2007**, *23*, 11421−11424.
(51) Liang, Z.; Liu, Y.; Ng, S. S.; Li, X.; Lai, L.; Luo, S.; Liu, S. The Effect of pH Value on the Formation of Gold Nanoshells. *J. Nanopart. Res.* **2011**, *13*, 3301−3311.
(52) Kuzmenko, I.; Kindermann, M.; Kjaer, K.; Howes, P. B.; Als-Nielsen, J.; Granek, R.; Kiedrowski, G. v.; Leiserowitz, L.; Lahav, M. Crystalline Films of Interdigitated Structures Formed via Amidinium−Carboxylate Interactions at the Air−Water Interface. *J. Am. Chem. Soc.* **2001**, *123*, 3771−3783.
(53) Song, H.-M.; Wei, Q.; Ong, Q. K.; Wei, A. Plasmon-Resonant Nanoparticles and Nanostars with Magnetic Cores: Synthesis and Magnetomotive Imaging. *ACS Nano* **2010**, *4*, 5163−5173.
(54) Li, J.; Wu, J.; Zhang, X.; Liu, Y.; Zhou, D.; Sun, H.; Zhang, H.; Yang, B. Controllable Synthesis of Stable Urchin-like Gold Nanoparticles Using Hydroquinone to Tune the Reactivity of Gold Chloride. *J. Phys. Chem. C* **2011**, *115*, 3630−3637.
(55) Chen, S.; Wang, Z. L.; Ballato, J.; Foulger, S. H.; Carroll, D. L. Monopod, Bipod, Tripod, and Tetrapod Gold Nanocrystals. *J. Am. Chem. Soc.* **2003**, *125*, 16186−16187.
(56) Sreeprasad, T. S.; Samal, A. K.; Pradeep, T. Body- or Tip-Controlled Reactivity of Gold Nanorods and Their Conversion to Particles Through Other Anisotropic Structures. *Langmuir* **2007**, *23*, 9463−9471.
(57) Wu, H.-Y.; Liu, M.; Huang, M. H. Direct Synthesis of Branched Gold Nanocrystals and Their Transformation into Spherical Nanoparticles. *J. Phys. Chem. B* **2006**, *110*, 19291−19294.
(58) Niidome, T.; Yamagata, M.; Okamoto, Y.; Akiyama, Y.; Takahashi, H.; Kawano, T.; Katayama, Y.; Niidome, Y. PEG-Modified Gold Nanorods with a Stealth Character for in Vivo Applications. *J. Controlled Release* **2006**, *114*, 343−347.
(59) Takahashi, H.; Niidome, Y.; Niidome, T.; Kaneko, K.; Kawasaki, H.; Yamada, S. Modification of Gold Nanorods Using Phosphatidylcholine to Reduce Cytotoxicity. *Langmuir* **2005**, *22*, 2−5.
(60) Jackson, J. B.; Halas, N. J. Surface-Enhanced Raman Scattering on Tunable Plasmonic Nanoparticle Substrates. *Proc. Natl. Acad. Sci. U. S. A.* **2004**, *101*, 17930−17935.
(61) Zhang, P.; Guo, Y. Surface-Enhanced Raman Scattering Inside Metal Nanoshells. *J. Am. Chem. Soc.* **2009**, *131*, 3808−3809.
(62) Ochsenkühn, M. A.; Jess, P. R. T.; Stoquert, H.; Dholakaia, K.; Campbell, C. J. Nanoshells for Surface-Enhanced Raman Spectroscopy in Eukaryotic Cells: Cellular Response and Sensor Development. *ACS Nano* **2009**, *3*, 3613−3621.
(63) Rodríguez-Lorenzo, L.; Krpetic, Z.; Barbosa, S.; Alvarez-Puebla, R. A.; Marzán, L. M.; Prior, I. A.; Brust, M. Intracellular Mapping with SERS-Encoded Gold Nanostars. *Integrative Biol.* **2011**, *3*, 922−926.